USING GEOGRAPHIC INFORMATION SYSTEMS (GIS) AND REMOTE SENSING TO MAP FLOOD EXTENT AND TO ASSESS FLOOD HAZARD IN ERYTHROPOTAMOSRIVER BASIN (EVROS, GREECE).

[1]Domakinis C., [1]Oikonomidis D., [2]Voudouris K., [1]Astaras T.

[1] *Aristotle University of Thessaloniki, Faculty of Science, School of Geology, Department of Physical and Environmental Geography, Thessaloniki 54124, Greece*

[2]*Aristotle University of Thessaloniki, Faculty of Science, School of Geology, Department of Geology, Thessaloniki 54124, Greece*

Abstract

According to 2007/60/EC Directive of the European Parliament and the Council of the European Union, floods are recognised as a phenomenon that causes severe damage upon both the environment and mankind. Having this Directive in mind, the present study focuses on the flood of the river basin of the tributary river of Evros called Erythropotamos. Also, taking under consideration that the event occurredbetween the 9thand 18th of February in 2010 in this area, this preliminary study attempts to achieve detection and mapping of its extent, along with determining if there is a connection between the latter and the geologic formations of the study area. Moreover, data layers such as land cover, hydrogeology, topography and EU-DEM's 1 arc second (approximately 25m) spatial resolution elevation data, were used in order to achieve hazard assessment in Erythropotamos' catchment with the aid of Hec-RAS software and its ArcGIS extension HEC-GeoRAS by compiling flood hazard and risk maps. Finally, these maps were evaluated by comparingthe flood extent depicted in them with the flood extent that was initially mapped with ENVISAT imagery by usingmeasures of fit tests. The results evaluated the existing methodologies for their effectivenessand accuracy to achieve flood risk assessment mapping and raise the question if there are ways in which these results can be improved.

Keywords: Geology, Geography, Floods, GIS, Remote Sensing, HEC RAS

1. Introduction

Flooding is a very common environmental hazard with over 3,000 disasters recorded in the Centre for Research on the Epidemiology of Disasters (CRED) database since 1900. This is because of the widespread distribution of river floodplainsand low-lying coasts and their long-standing attractions for human settlement. Each year, floods claim around 20,000 lives and adversely affect at least 20 million people worldwide, mostly through homelessness (Smith & Petley, 2009).

In order to mitigate the severe damage that floods cause upon the environment and mankind, remote sensing and airborne systems, were initially employed in order to study such phenomena because they provided cost-effective spatially distributed data over large areas. An early attempt was performed by Lowry, that used a side-looking airborne radar at X- and L-bands to map the Manitoba flood of 1979 (Pulvirenti et al., 2011 from Lowry et al., 1981). Traditional airphoto interpretation has long been utilized to map floodplain environments. While useful it lacked the spectral dimensions of data derived from sensors (Hudson et al., 2003). Since the beginning of the satellite era in the 1960s, mankind has been trying to map large scale floods using remotely sensed data from optical sensors of Landsat –TM5, Landsat –ETM7, NOAA's AVHRR sensors, MODIS, ASTER and synthetic aperture radar (SAR) sensors of European Remote Sensing Satellites (ERS-1 and ERS-2), ENVISAT, Canadian Radarsat-1, and Radarsat-2 and the Japanese JERS-1 and JERS-2 (Gan et al., 2012 from Hess et al., 1995; Wang et al., 1995; Bates, 2004; Bates and De Roo, 2000; Jodouin et al., 2003; Horritt, 1999, 2006), and sometimes at global scale (Prigent et al., 2007). These efforts came to the conclusion that optical sensors are weather dependent, and cloudy conditions could prevent themfrom identifying flooded areas from such satellite data. On the other hand, radar sensors are weather independent, but, unlike visual interpretation of flooded areas from images acquired from optical sensors, interpretation of SAR images involves more ambiguities. For example, speckles and pixel values of SAR images are dependent not only on the dielectric constant ε (due to water), but also on surface roughness, geometric distortions, layover effects, and other factors. Even though a wet surface could appear bright because of high surface roughness, it generally appears dark, because when soil gets wet, its ε increases substantially to about 30 (Gan et al., 2012 from Hendrickx et al., 2003). The brightness of a SAR image also depends on the incidence angle, surface roughness and polarization. Typically for flood mapping (smooth surface), copolarization (HH or VV) has a 0° phase difference and so is preferred over cross-polarization (VH or HV) which has a phase difference uniformly distributed between -180° and +180°, and so the latter does not contain much target-specific information (Gan et al., 2012).

Until nowadays, many different methods were proposed to flood extent extraction from satellite imagery. European Space Agency (ESA) suggests a multi-temporal technique that uses SAR images of the same area taken on different dates (one image is acquired during flooding and the second one in “normal” conditions). The resulting multi-temporal image clearly reveals change in the Earth’s surface by the presence of colour in the image. Cunjian et al. (2001) applied threshold segmentation algorithm to flood extent extraction from RADARSAT-1 imagery with the support of digital topographic data. The drawback of this approach is that threshold value should be chosen manually, and will be specific for different SAR instruments and images. Csornai et al. (2004) used ESA’s ERS-2 SAR images and optical data (Landsat TM, IRS WIFS/LISS, NOAA AVHRR) for flood monitoring in Hungary in 2001. To derive flood extent from SAR imagery, change detection technique is applied. This technique uses two images made before and during the flood event, and some “index” that reveals changes in two images and, thus, the presence of water due to the flooding (Kussul et al., 2008 from Wang, 2002). Though these methods are rather simple and fast (in computational terms), they possess some disadvantages: they need manual threshold selection and image segmentation, require expertise in visual interpretation of SAR images and require the use of complex models for speckle reduction; spatial connections between pixels are not concerned. Further sophisticated approaches have been proposed to segment SAR imagery for flood and coastal applications by Horritt, 1999; Niedermeier et al., 2000; Dellepiane et al., 2004; Martinez and Le Toan, 2007; Kussul et al., 2008.

Along with remote sensing technology, the Geographic Information Systems (GIS) have become a key tool for flood mapping and flood risk assessment (Sanyal and Lu, 2004; Dewan et al., 2007) because GIS provide a broad range of tools for determining the flood affected area and for forecasting areas that are likely to be flooded due to a high water level (Islam and Sado, 2000; Sarma, 1999).

Between 1998 and 2004, Europe suffered over 100 major damaging floods, including the catastrophic floods along the Danube and Elbe rivers in summer 2002. Severe floods in 2005 further reinforced the need for concerted action. As a result, the European Commission published the so called Flood Directive (2007/60/EC) on the assessment and management of flood risks in 2007 and theEuropean Parliament along with the Council of the European Union adopted it. According to the aforementioned Directive, theMember States of the European Community were urged to compile flood hazard and risk maps in order to complete a preliminary flood risk assessment that will further aid in alleviating the adverse consequences of floods for their countries. Particularly, flood hazard maps include the extent of flooding (inundation mapping) for a given flood recurrence interval, and other fundamental hydraulic information such as flood depth, velocity and frequency of inundation (Alcantara – Ayala & Goudie, 2010 from Wolman, 1971). On the other hand, flood risk maps illustrate the area of inundation and the potential damage impact, including human risk, economic value and impacts on environmental systems (Alcantara – Ayala & Goudie, 2010). The aforementioned definitions for hazard and risk maps are in accordance with the framework provided by the 2007/60/EC Directivethat clearly specifies the content of such maps, which was a matter of debate before this Directive came into effect.Furthermore, remotesensing and GIS are widely considered as invaluable tools in the compilation of such maps with their vast range of processing and mapping capabilities.

In Greece, river Evros, which is the natural borderline between Greece and Turkey, frequently bursts its banks and inundates its surrounding area damaging nearby farmlands and sometimes even causing the loss of human lives. Erythropotamos River (Fig. 1) is one of Evros' tributaries and heavy rainfall caused it to flood an area of more than 140,000 acres, according to local media information, from 9th to 18th of February in 2010. As a result, villages were evacuated and properties were damaged to such extent that local authorities found it difficult to estimate the amount of money that they would have to spend in order to refund those who were affected by the phenomenon.

The aim of this study, which involves the preliminary results of a PhD thesis, is to use initially remote sensing SAR imagery in order to delineate the extent of the area within Erythropotamos' catchment that was inundated during the aforementioned flood event. Furthermore, it tries to find out if geology can be related with the flooded area and if certain lithological formations of the study area favour the concentration of rainfall water. Additionally, the present study uses the 1D hydrological modelling software HEC-RAS (Hydrologic Engineering Center – River Analysis System) and its ArcGIS extension HEC-GeoRAS in order to compile flood risk and hazard maps for Erythropotamos' main watercourse according to 2007/60/EC Directive standards andit utilizes measure of fit tests in order to evaluate their accuracy.

2. Study area

2.1 Location of the study area

As mentioned above, Erythropotamos is one of the many tributaries of Evros River and its catchment covers an extent of 1,609.228 km^2, which mostly belongs to Greece and particularly to the geographic region of Thrace in Northern Greece. The rest of its drainage basin belongs to Bulgaria. (Fig.1). Regarding administrative distribution, the Greek part of Erythropotamos' river basin belongs to the Counties of Evros and Rhodopi.

2.2 Geology, geomorphology and hydrogeology of the study area

The study area belongs to the Circum - Rhodope geotectonic zone and the Rhodope massif.The geological formations within the extent of Erythropotamos' catchment consist mostly of gneiss, pegmatites, marbles, amphibolites and sediments (Fig. 2). Table 1 contains a detailed description of the river basin's lithological composition. Elevation in the study area ranges from 15 m to 1,258 m (Fig. 3), while the surface, based on GIS elevation data, can be described as hilly, according to Dikau's classification (Dikau, 1989), due to the fact that elevation ranging from 150 m to 600 m covers 59.8% of the area (Tab.2) (Domakinis et al., 2008).

According to a study that was carried out for a water dam that was built in the village of Mikro Dereio, the mean annual discharge and mean discharge, derived from gauges at that location, were 202,800,000 m^3 and 6.43 m^3/s, respectively (Bezes, 1994). Additionally, with the aid of ArcGIS software the main water course of Erythropotamos was measured to be 104.17km in length and the drainage system's highest Strahler stream order is that of the 6th order (Fig. 1).

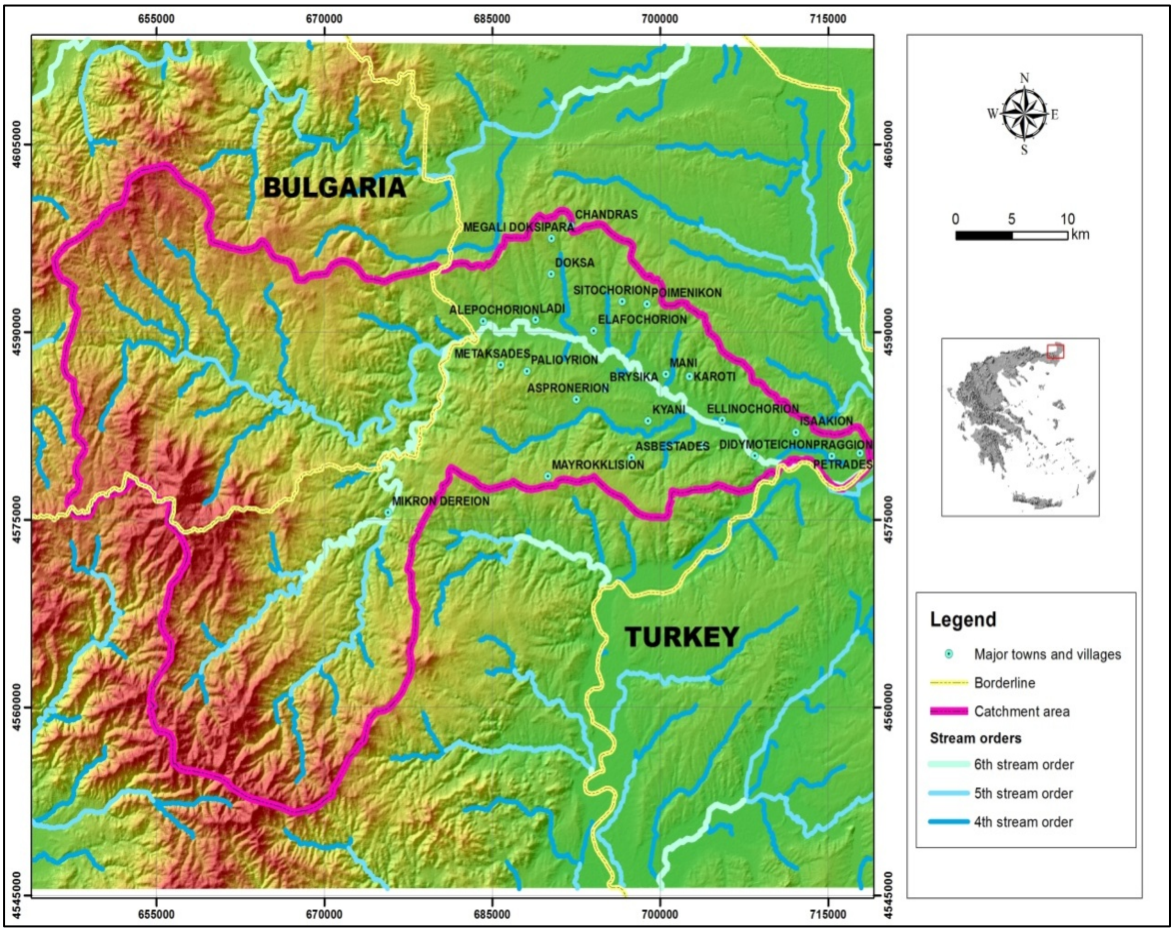

Figure 1: The catchment (study area of Erythropotamos River along with its drainage network).

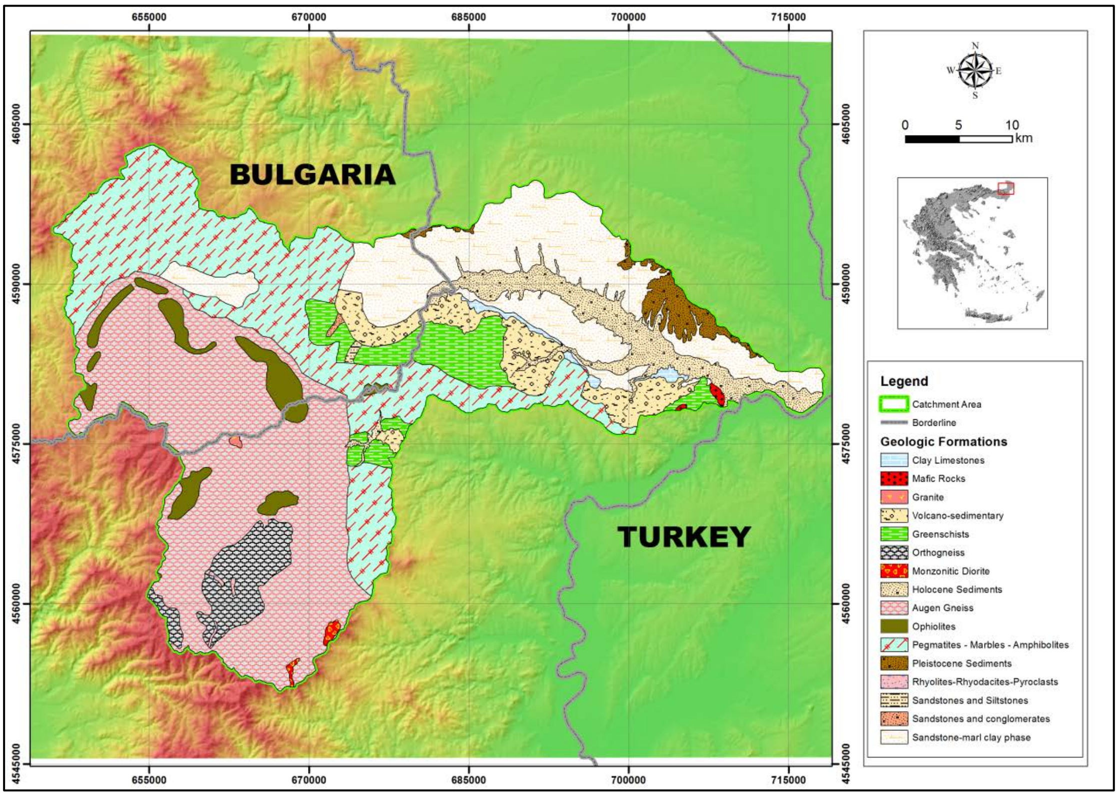

Figure 2: Geological map of the study area.

Geological Formation	Area (km^2)	Percent (%)
Clay Limestone	9.56	0.594
Mafic Rocks	1.99	0.124
Granite	0.956	0.059
Volcano-sedimentary	88.735	5.514
Green schists	86.628	5.383
Orthogneiss	61.201	3.803
Monzonitic Diorite	3.247	0.202
HoloceneSediments	95.679	5.946
Augen Gneiss	498.17	30.957
Ophiolites	54.651	3.396
Pegmatites - Marbles - Amphiblites	386.187	23.998
Pleistocene Sediments	30.457	1.893
Rhyolites - Rhyodacites - Pyroclasts	1.714	0.107
Sandstones & Siltstones	1.696	0.105
Sandstones & Conglomerates	1.292	0.080
Sandstone-marlclayphase	287.065	17.839

Table1: Geological formations of Erythropotamos' catchment area.

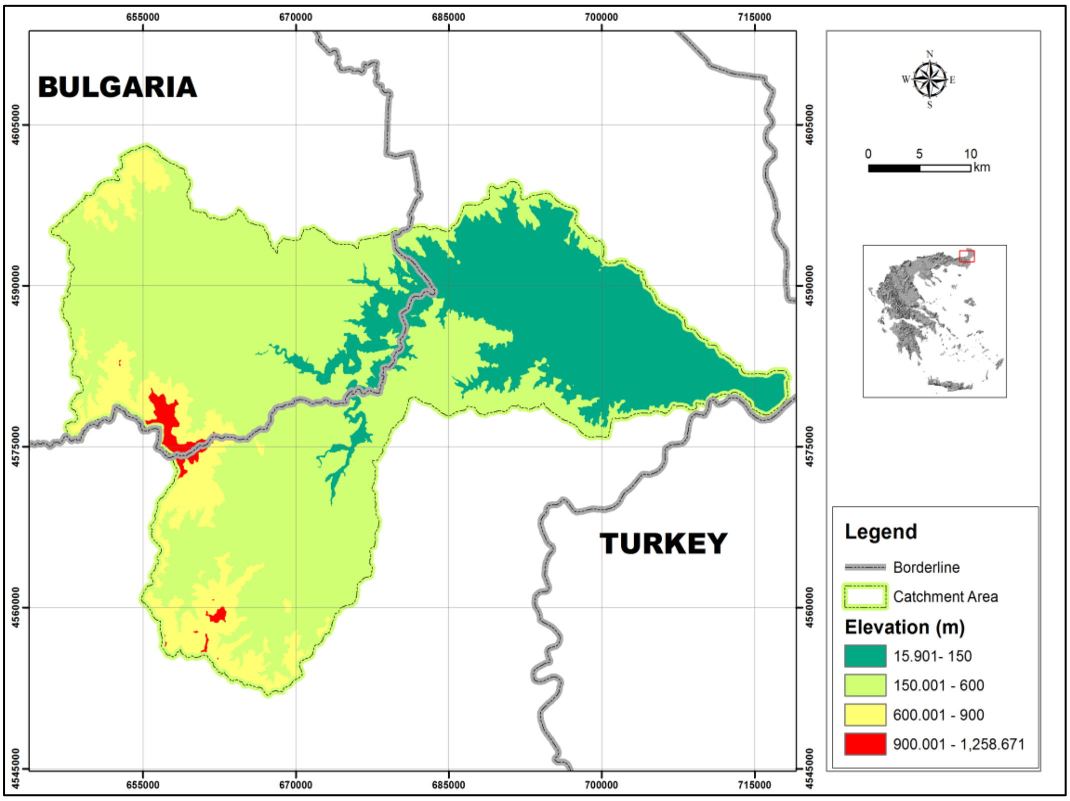

Figure 3: Elevation categories according to Dikau's classification.

Elevation	Description	Area (km^2)	Percent (%)
<150	Lowland	432.641	26.885
150-600	Hilly	963.371	59.865
600-900	Semi-mountainous	192.447	11.959
900>	Mountainous	20.769	1.291

Table2: Eleveation categories according to Dikau's classification.

3. Materials and Methodology

3.1 Satellite data and floodplain delineation

Satellite SAR data, and particularly ENVISAT/ASAR images of VV (Vertical-Vertical) polarisation, which were taken from the year 2002 up to the year 2010, were acquired through the submission of a CAT-1 proposal to ESA (European Space Agency), for the completion of a PhD thesis. These images were calibrated, despeckled, coregistered and orthorectified with the aid of ESA's SAR satellite image analysis software NEST (Next ESA SAR Toolbox) (Mouratidis, 2011).

Having tried a number of methodologies for floodplain delineation, ESA's methodology was finally selected in order to discern the inundated areas. According to ESA's suggested methodology for flood mapping NEST can be used in order to create RGB images whose combination enables us to distinguish between areas that are flooded and permanent water bodies. This can be achieved by using one SAR image that was acquired during the flood event (crisis image) and another (archive image) that is covering the same area. By placing the "crisis image" in the Red channel and the "archive image" in both the Green and Blue channels, in areas that are flooded, the red channel will be dark but the Green and Blue channels will be bright, therefore the pixels should appear bright cyan. Permanent water bodies will be dark in all channels, while all other areas should be a shade of grey as the backscatter intensity should be the same (E.S.A., 2008).

From the total of the ENVISAT/ASAR images that were obtained through the CAT-1 proposal to ESA, the image that was acquired on 16/2/2010 was chosen as the "crisis image" and the ENVISAT/ASAR image that was acquired on 23/12/08 was chosen as the "archive image". According to the meteorological and hydrological river gauges of the station near Didymoteicho, which provide data at a 50 minute intervals. When deep bare soil areas are flooded, their backscattering is highly dependent on the wind-induced surface roughness at steep incidence angles.

Backscattering values have been compared with the wind velocity averaged for the 6 hours prior to image acquisition, which is the wind responsible for the water surface roughness at that time, and the results showed that above a mean wind velocity of about 1.5 m/s there is a positive correlation between wind speed and σ° (sigma nought/scattering coefficient) (Marti-Cardona et al., 2010). During the date and time that both images were acquired, wind speed did not exceed 1.5 m/s, so the water surface of the river could be considered as calm. Moreover, in order to track soil moisture dynamics, using change detection methods, the historically "driest" image is normally used as the reference (or archive) image (Hostache et al., 2012). Discharge of Erythropotamos River during the acquisition time of the 'archive image' was measured at 0.65 m^3/s, thus indicating dry conditions, which are favourable for such an image.

According to ESA, good threshold values for flooded areas (for amplitude SAR images) could be those less than 800 for the "crisis image" and those more than 900 for the "archive image"

(E.S.A., 2008). Having that in mind, both the "crisis" and the "archive" image were converted into amplitude images and the flooded areas were extracted via thresholding (Fig. 4).

3.2 Floodplain delineation and geology

The synoptic geologic map of SE Rhodope – Thrace from the Institute of Geology and Mineral Exploration of Greece, at a scale of 1:200,000, was used in order to produce the data layer for the part of the geologic formations that belongs to Greece. Accordingly, the geologic map of Bulgaria from the Committee of Geology (Department of Geophysical Prospecting and Geological Mapping), at a scale of 1:50,000, which was compiled on the base of the Geological map of Bulgaria at a scale of 1:100,000, was used in order to produce the data layer for the part of the geologic formations that belongs to Bulgaria.

Following that, the data layer of the delineated flooded area was superimposed on the data layer of geology in order to discern, with the aid of ArcGIS' geoprocessing tools, if the aforementioned inundated areasare located upon certain lithological formations of the study area.

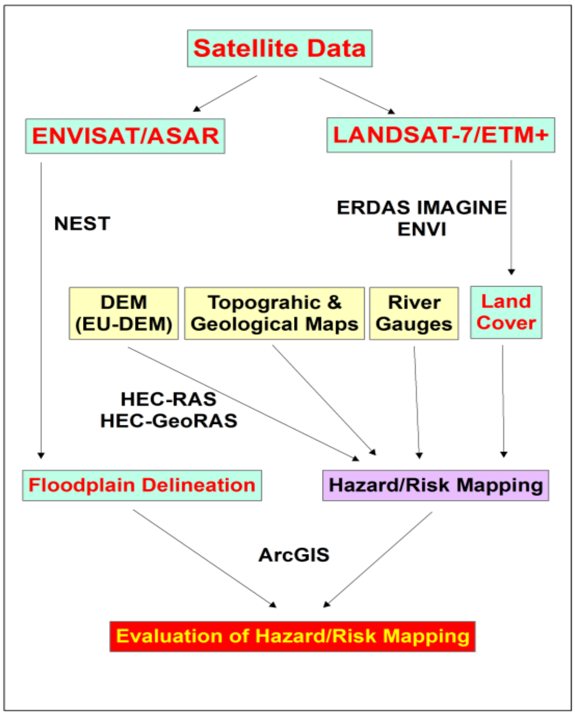

Figure 4: Flow diagram of the methodology that was used for the compilation and evaluation of flood hazard and risk maps.

3.3 Satellite data and Land Cover map

Landsat-5/TMsatellite multi-spectral imagery was acquired free of charge from GLOVIS (U.S.G.S., 2011) internet site. Specifically, the satellite image that was acquired during 1/5/2010 was selected because it was the one closer to the day that the "crisis image" was acquired and also because there were no areas covered by clouds in it.

With the aid of satellite image analysis software Erdas Imagine and ENVI, the image mentioned above was classified using the Maximum Likelihood algorithm into the following categories, which are based upon the Corrine Land Cover 2000 classification system: 1) artificial surfaces, 2) non-irrigated arable land, 3) permanently irrigated land, 4) Grassland – pastures, 5) forests and 6) water bodies.

3.4 Flood Hazard/Risk Mapping

First of all, topographic maps at a scale of 1:50,000 from HMGS (Hellenic Military Geographical Service) were used along with geological maps of the same scale from IGME (Institute of Geology and Mineral Exploration) in order to examine the general geological and geomorphologic background of the study area (Voudouris, 2007). Following that, the data layers of Erythropotamos' main water course, bank lines, flow paths and cut lines were prepared via HEC-RAS's extension for ArcGIS, HEC-GeoRAS. Elevation data were provided by The Digital Elevation Model over Europe from the GMES RDA project (EU-DEM) (E.S.A., 2014), which is a Digital Surface Model (DSM) representing the first surface as illuminated by the sensors. The EU-DEM dataset is a realisation of the Copernicus programme, managed by the European Commission, DG Enterprise and Industry. Its horizontal spatial resolution is 1 arc second (approximately 25 m), while its absolute and relative vertical accuracy are 3.6 m and 5.3 m, respectively (Mouratidis & Ampatzidis: in press). Also, Manning's n coefficients were extracted from the Land Cover map that was produced on an earlier stage of the study.

The hydrological modelling software HEC-RAS utilizes geometry, land cover and topographic data in order to calculate water surface profiles for sections that are located along the path of a river watercourse, according to certain discharge values.In accordance to that procedure, the aforementioned data layers were imported in the hydrological modelling software HEC-RAS, where steady flow analysis was performed according to 2007/60/EC Directive standards for flood events of: 1) low probability (500 years), 2) medium probability (100 years) and 3) high probability (50 years). Additionally, steady flow analysis was carried out for the value of discharge that was gauged by the station near Didymoteicho during the acquisition date of the "crisis image". The analysis produced risk maps regarding environmentally protected areas that belong to Natura 2000 Network and hazard maps for water depth and inundation, with the latter usedfor comparisonwith the flooded area that was extracted via SAR imagery analysis. Finally, the evaluation was conducted with the measure of fit (F) of the following mathematical formula:

$$F = \frac{A \cap B}{A \cup B} \times 100$$

The letter A stands for the inundated area derived from the SAR data and B stands for the inundated area predicted by the hydrological model HEC-RAS (Bates &Roo, 2000).

4. Results

The resulting multi-temporal radar image RGB (R: 16/2/2010 G: 23/12/2008 B: 23/12/2008) (Fig. 5) indicates the flooded areas with bright cyan colours and separates them from permanent water bodies that appear in dark tones. The flooded area covers an extent of 27,608 km^2. Spatially distributed data of a flood event, e.g.: water levels, would certainly help to enhance reliability of the resulting false color multi-temporal radar image, but are very difficult to gauge in the field, especially due to the risk of people being injured (Hostache et al., 2010).

The major part of the flooded area (41.31%) is located upon augen gneisses, and a smaller part (26.92%) is located upon a geologic formation that consists of pegmatites, marbles and amphibolites. Moreover, approximately 13% of the aforementioned flooded area is located upon Holocene sediments and another 5.07% appears upon a formation, which is composed by sandstone of marl-clay phase (Fig. 6, Table 3). Furthermore, cadastral orthophotos, with spatial resolution of 0.62 m, were used to assess the classification's accuracy. According to Erdas Imagine calculations, the overall classification accuracy for the resulting land cover map was 90.91% and kappa coefficient was 0.8638. Table 3 shows how the land cover types mentioned above extent throughout the catchment area of Erythropotamos (Fig. 7, Table 4).

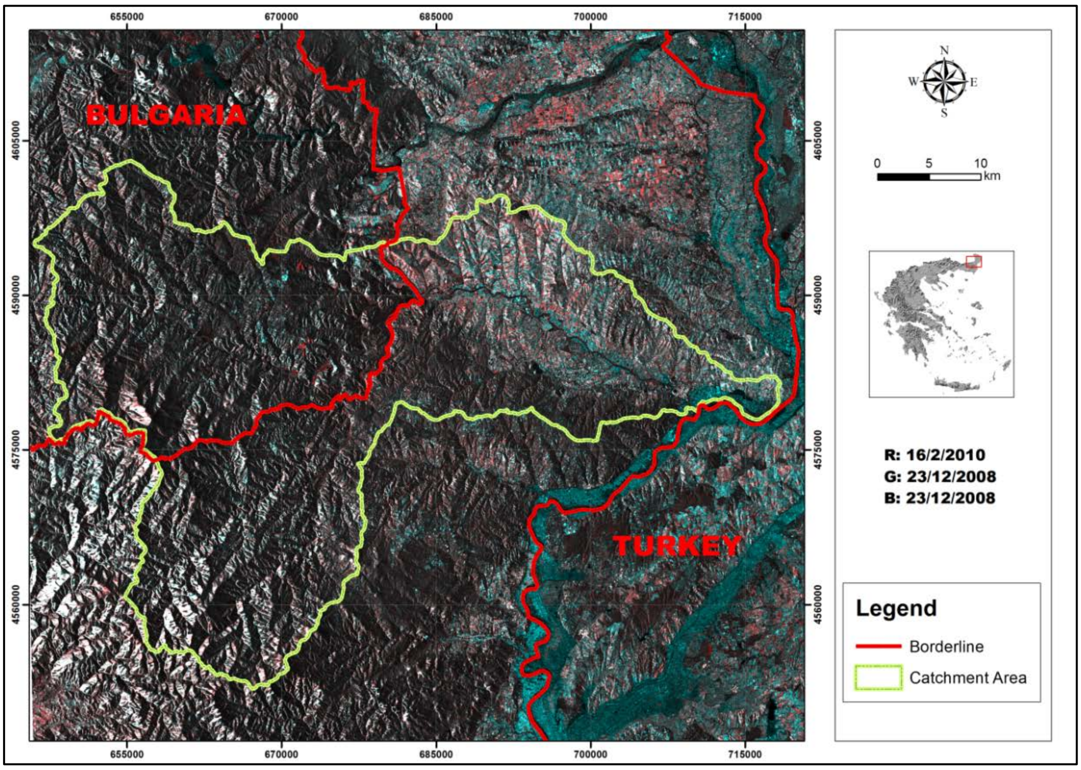

Figure 5: RGB: (16/2/2010, 23/12/2008, 23/12/2008) false color multitemporal radar image. In areas that are flooded, pixels appear bright cyan, while permanent water bodies appear in dark tones.

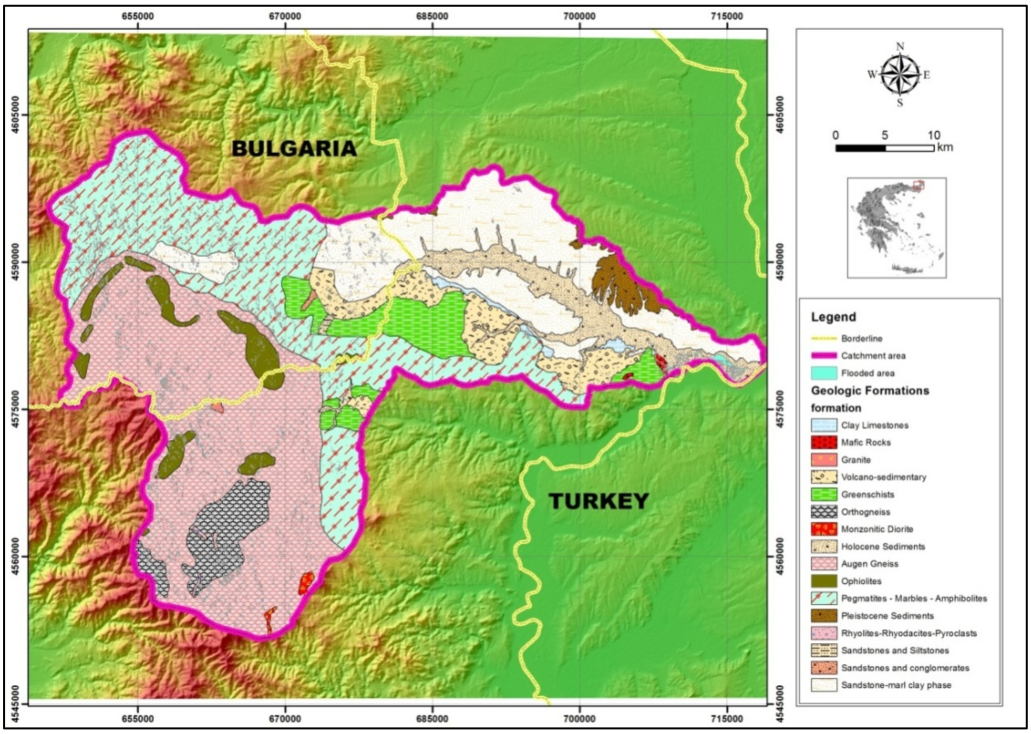

Figure 6: The flooded area that was delineated with the aid of ENVISAT/ASAR images is superimposed upon the data layer of geology of the study area.

Geological Formation	Area (km^2)	Percent (%)
Clay Limestone	0.085	0.31
Mafic Rocks	0.262	0.95
Granite	0.021	0.08
Volcano-sedimentary	0.403	1.46
Greenschists	0.475	1.72
Orthogneiss	1.182	4.28
Monzonitic Diorite	0.012	0.04
Holocene Sediments	3.585	12.99
Augen Gneiss	11.404	41.31
Ophiolites	1.249	4.52
Pegmatites - Marbles - Amphibolites	7.431	26.92
PleistoceneSediments	0.045	0.16
Rhyolites - Rhyodacites - Pyroclasts	0.022	0.08
Sandstones & Siltstones	0.03	0.11
Sandstones & Conglomerates	0.002	0.01
Sandstone-marlclayphase	1.4	5.07

Table 3: Distribution of the flooded area according to the geological formations of the study area.

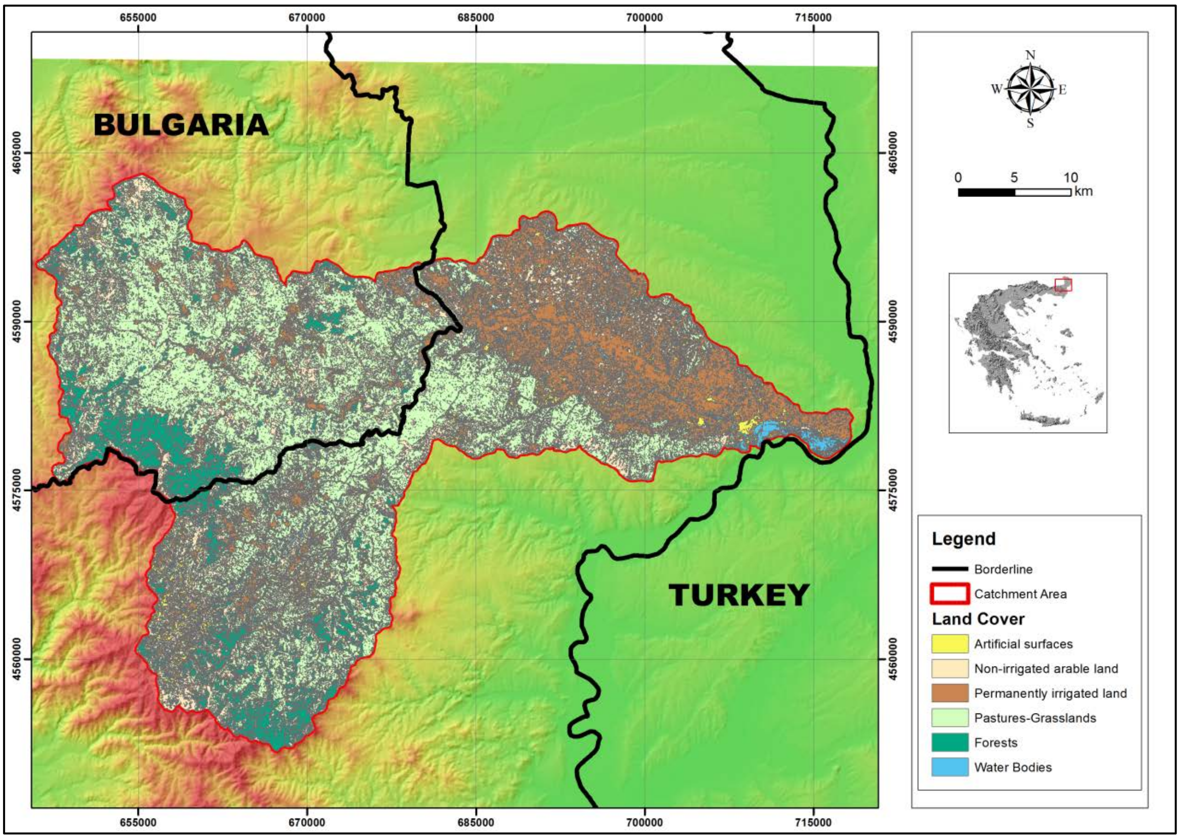

Figure 7: Land cover map of the study area.

Land Cover	Area (km^2)	Percent (%)
Artificial surfaces	48.085	2.988
Non-irrigated arable land	291.335	18.104
Permanently irrigated land	335.12	20.825
Grassland – pastures	740.65	46.025
Forests	148.273	9.214
Waterbodies	45.765	2.844

Table 4: Land Cover classification categories.

Flood hazard maps were compiled, as mentioned earlier, not only according to 2007/60/EC Directive standards for flood events with return period of 500 years,100 years and 50 years, but also for the value of discharge that was gauged by the station near Didymoteicho during the acquisition date of the “crisis image”. This discharge value corresponds to the 5 year return period in agreement with Giadotti’s mathematical formula (Soulios, 1996) for the calculation of flood discharge.

Having taken these parameters under consideration, the resulting flood hazard maps depicted the spatial extent for the hydraulic parameters of flood depth and inundation area. Figures 8, 9, 10 and 11 show water depths of the flooded area for the return periods of 5, 50,100 and 500 years respectively, while figures 12, 13, 14, and 15 show the extent of the modelled flooded area for the same return periods.

Additionally, flood risk maps (Figs 16, 17, 18 & 19) indicate the intersection between the areas that were predicted by the hydraulic model that was produced by HEC-RAS and the Special Protection Areas (SPA) that belong to Natura 2000. Specifically, these areas are GR1130011 (Valley of Filiouri) and GR1110010 (Valley of Dereion). The results from the compiled hazard and risk maps and their respective measures of fit are summed up on Table 5.

Return Period	Area (km^2)	Flood Depth (m)	Area intersecting with Natura 2000 (km^2)	Measure of fit (%)
5 years	36.931	17.4	5.424	1.2019
50 years	42.289	18.5	5.932	1.1885
100 years	43.371	18.8	6.057	1.1789
500 years	45.297	19.5	6.295	1.1768

Table 5: The results from the compiled hazard/risk maps and their respective measures of fit.

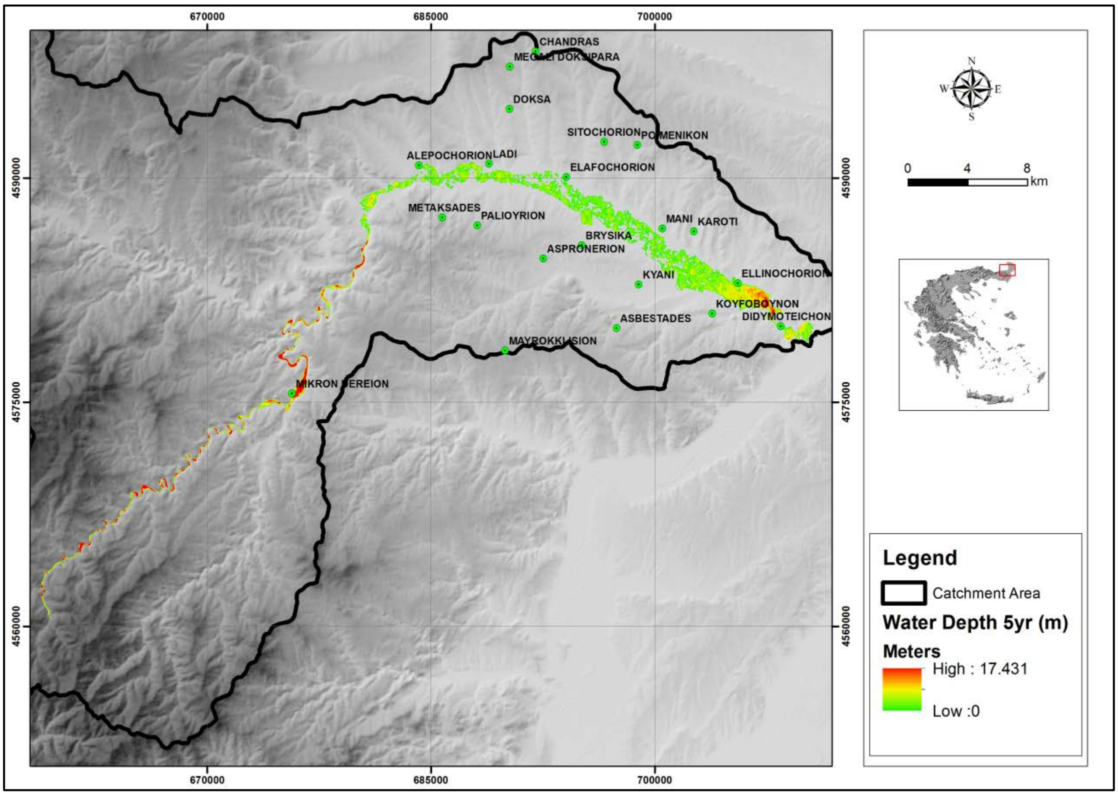

Figure 8: Flood hazard map which shows water depth in the inundated area for the return period of 5 years. Red colour indicates high values of water depth, while green indicates low values.

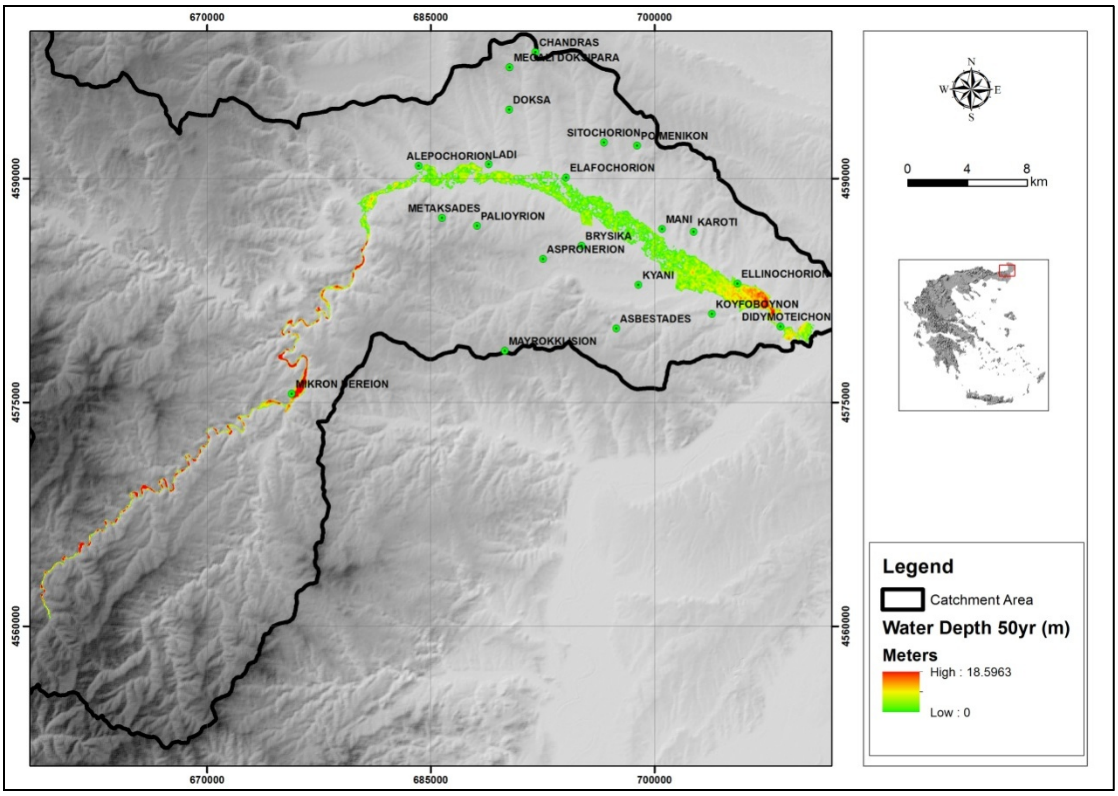

Figure 9: Flood hazard map which shows water depth in the inundated area for the return period of 50 years. Red colour indicates high values of water depth, while green indicates low values.

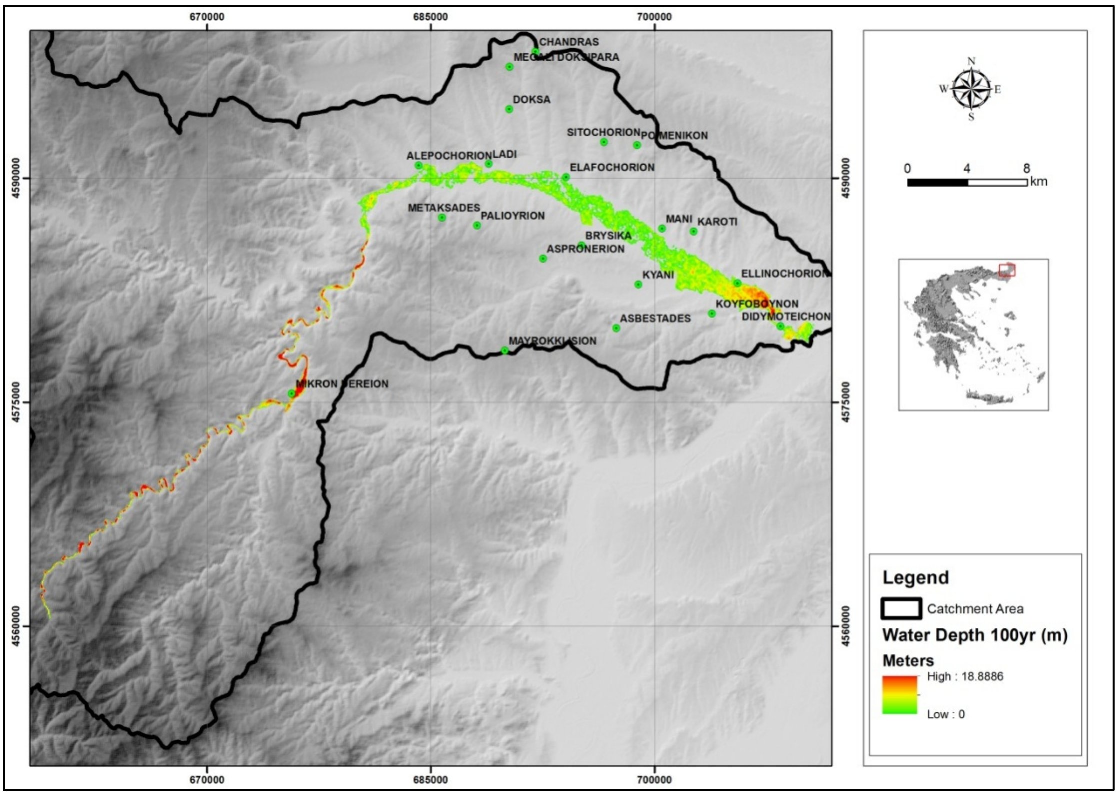

Figure 10: Flood hazard map which shows water depth in the inundated area for the return period of 100 years. Red colour indicates high values of water depth, while green indicates low values.

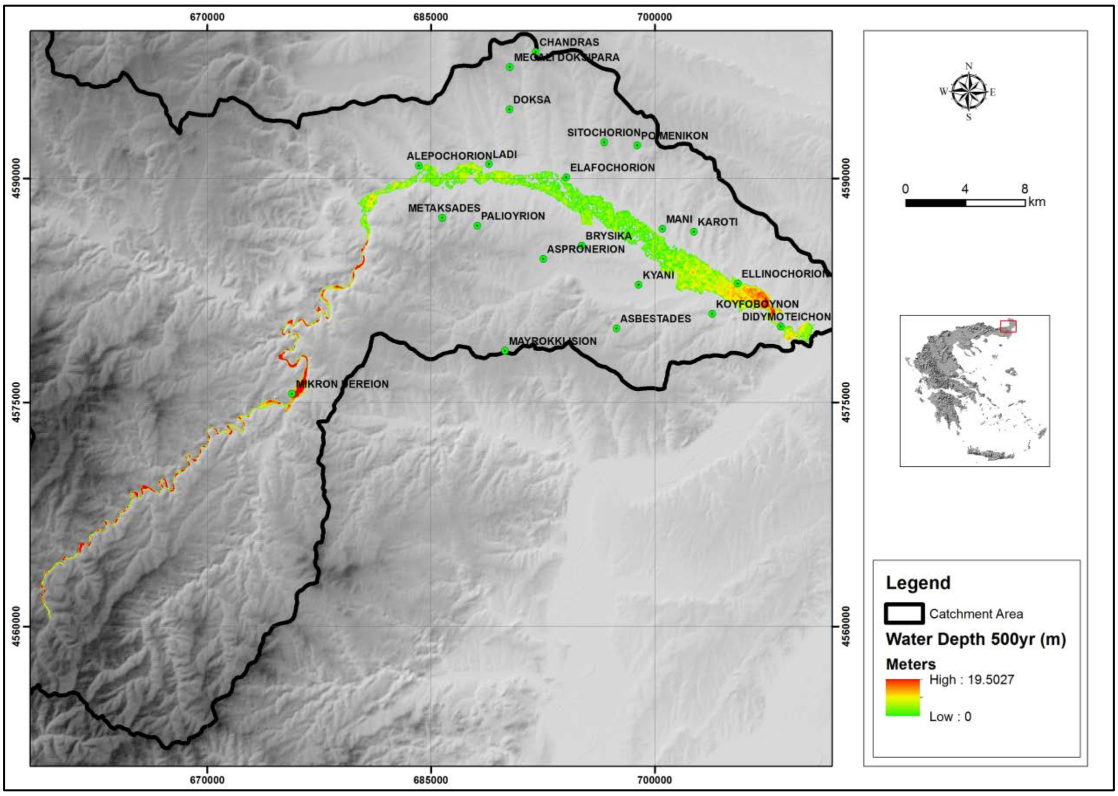

Figure 11: Flood hazard map which shows water depth in the inundated area for the return period of 500 years. Red colour indicates high values of water depth, while green indicates low values.

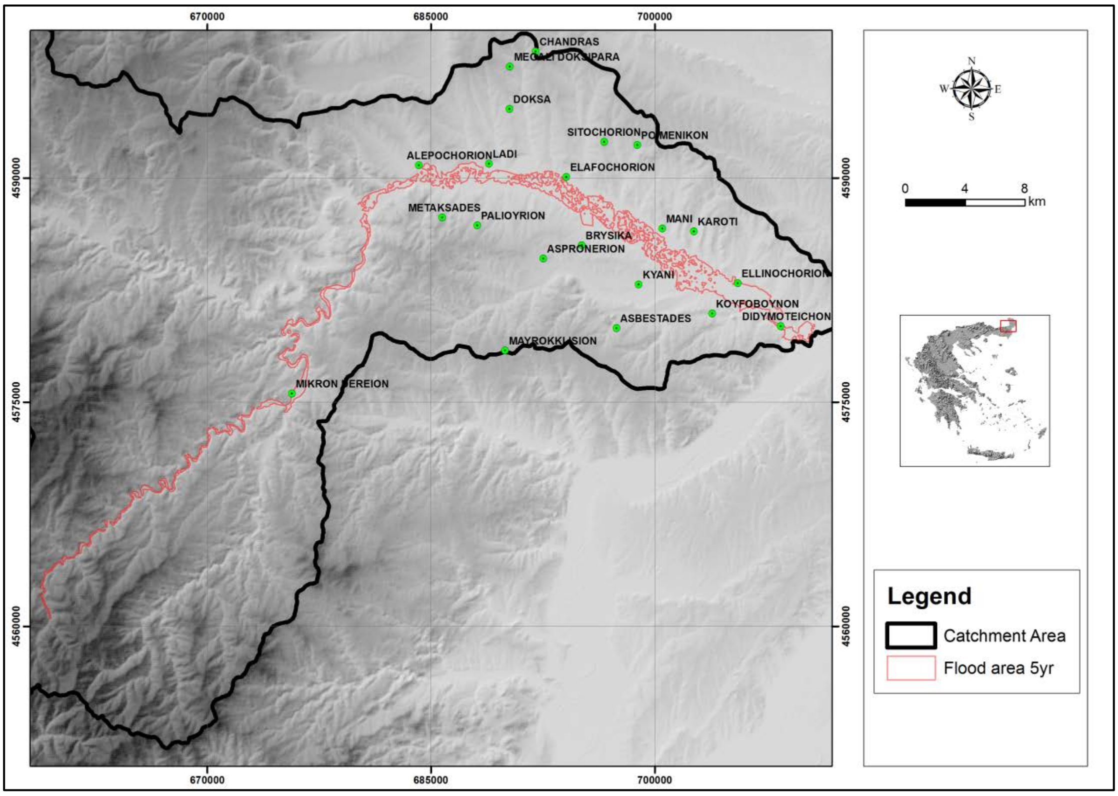

Figure 12: Flood hazard map which shows the inundated area for the return period of 5 years.

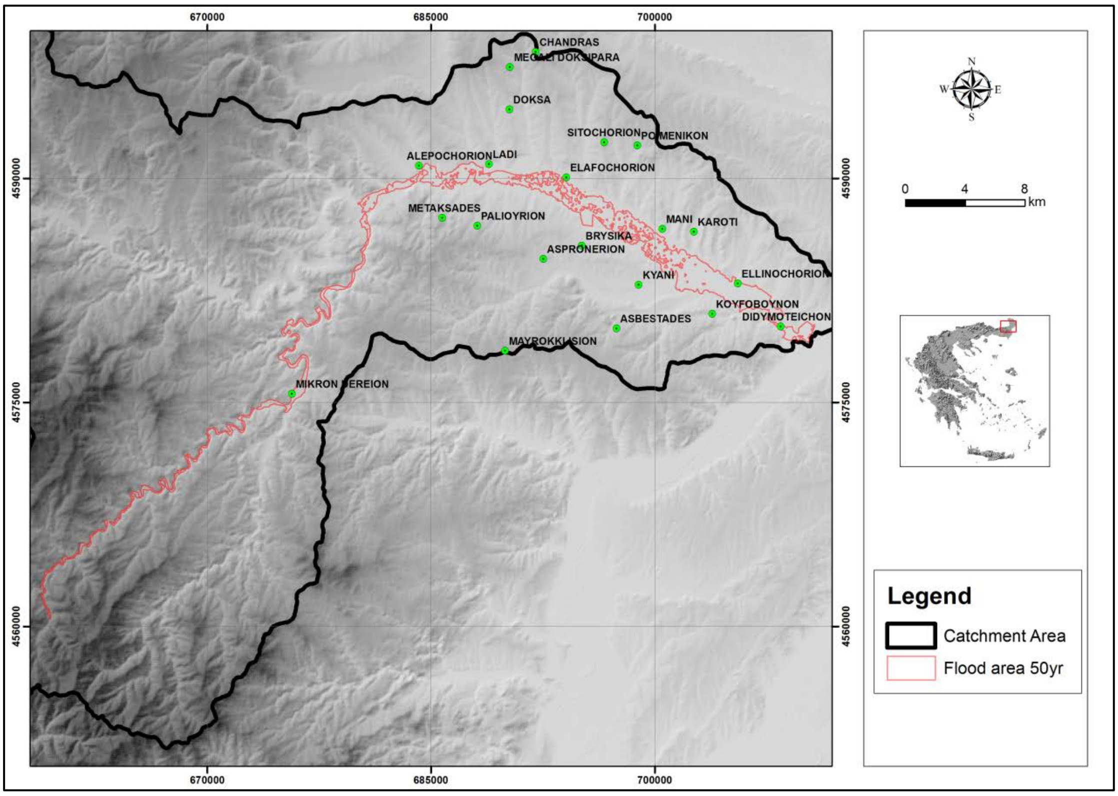

Figure 13: Flood hazard map which shows the inundated area for the return period of 50 years.

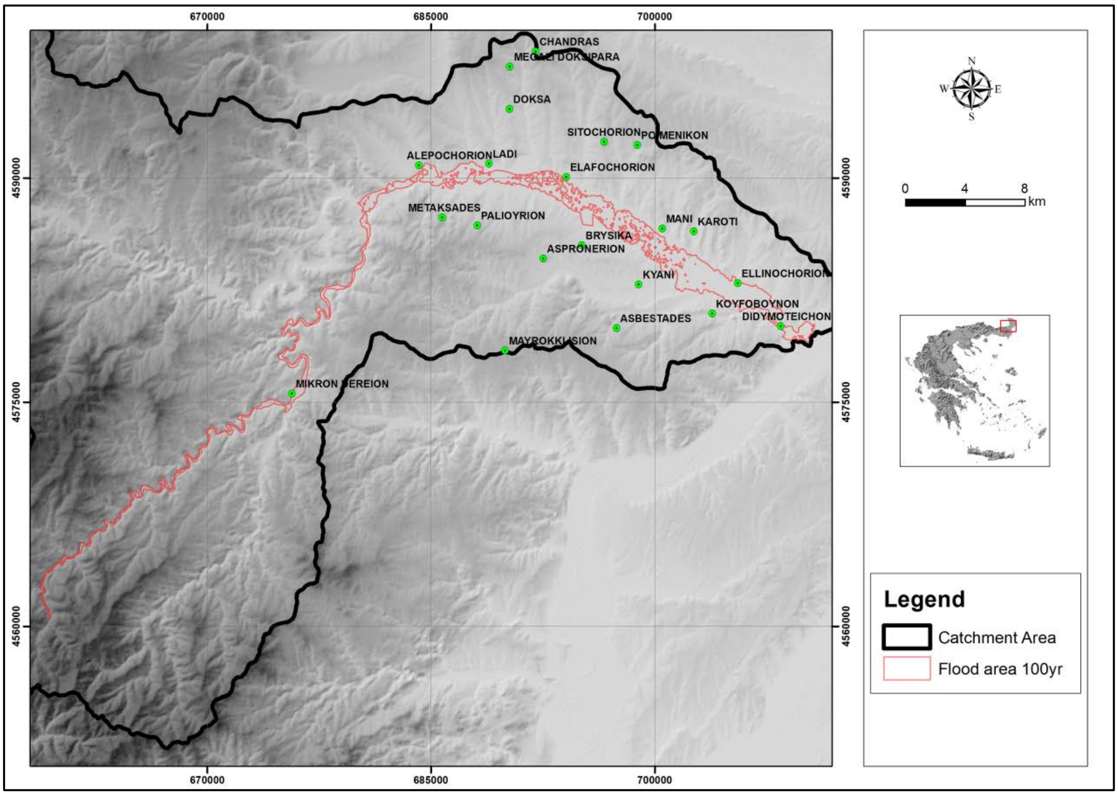

Figure 14: Flood hazard map which shows the inundated area for the return period of 100 years.

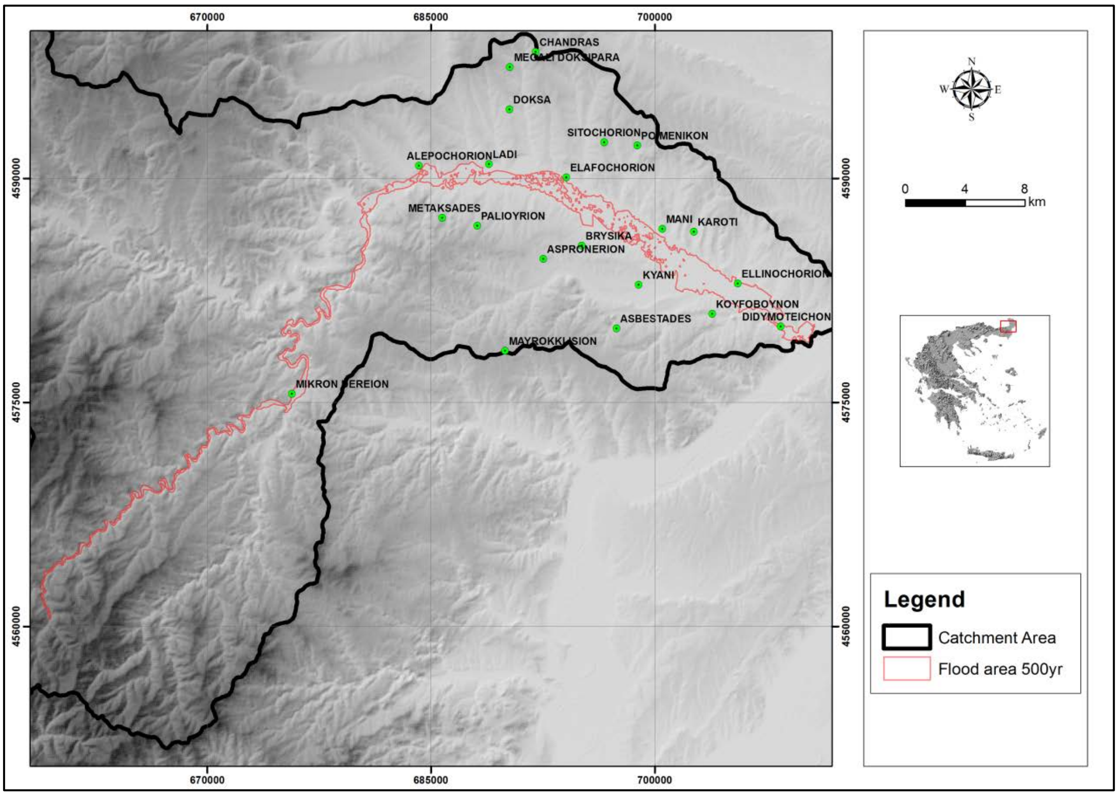

Figure 15: Flood hazard map which shows the inundated area for the return period of 500 years.

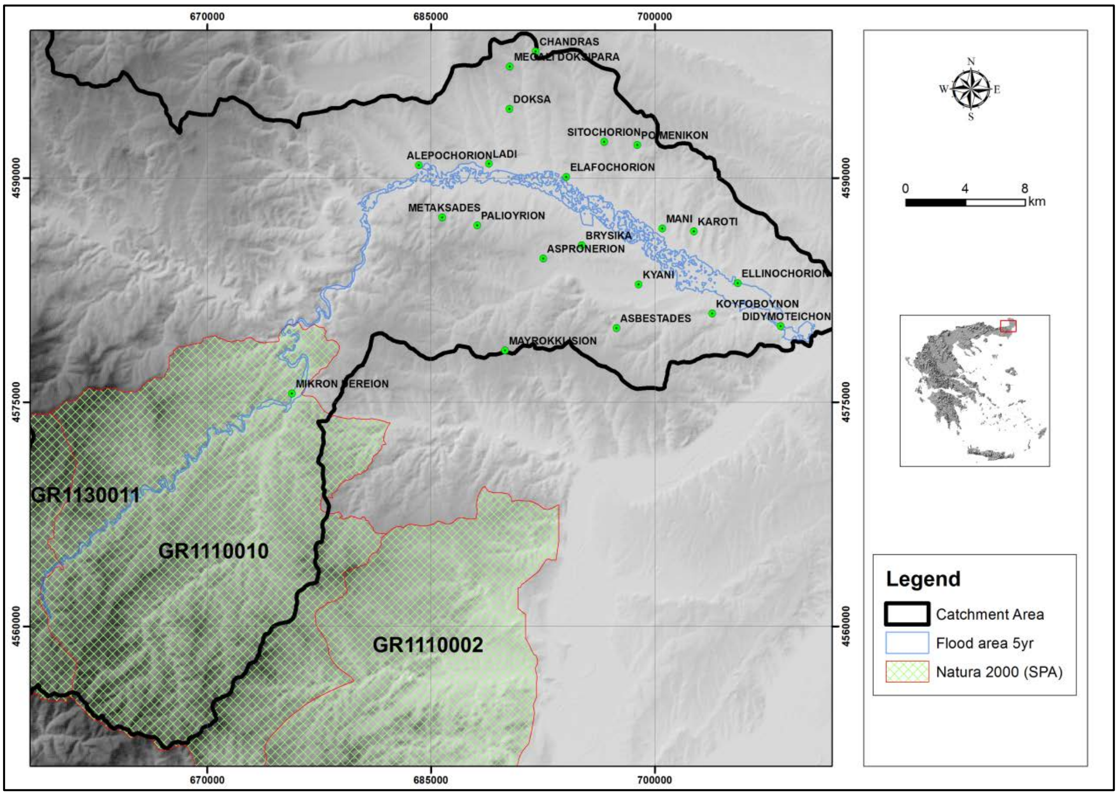

Figure 16: Flood risk map depicting the intersection between the inundated area of the 5 year period and Natura 2000 protected areas (GR1130011: Valley of Filiouri, GR1110010: Valley of Dereion).

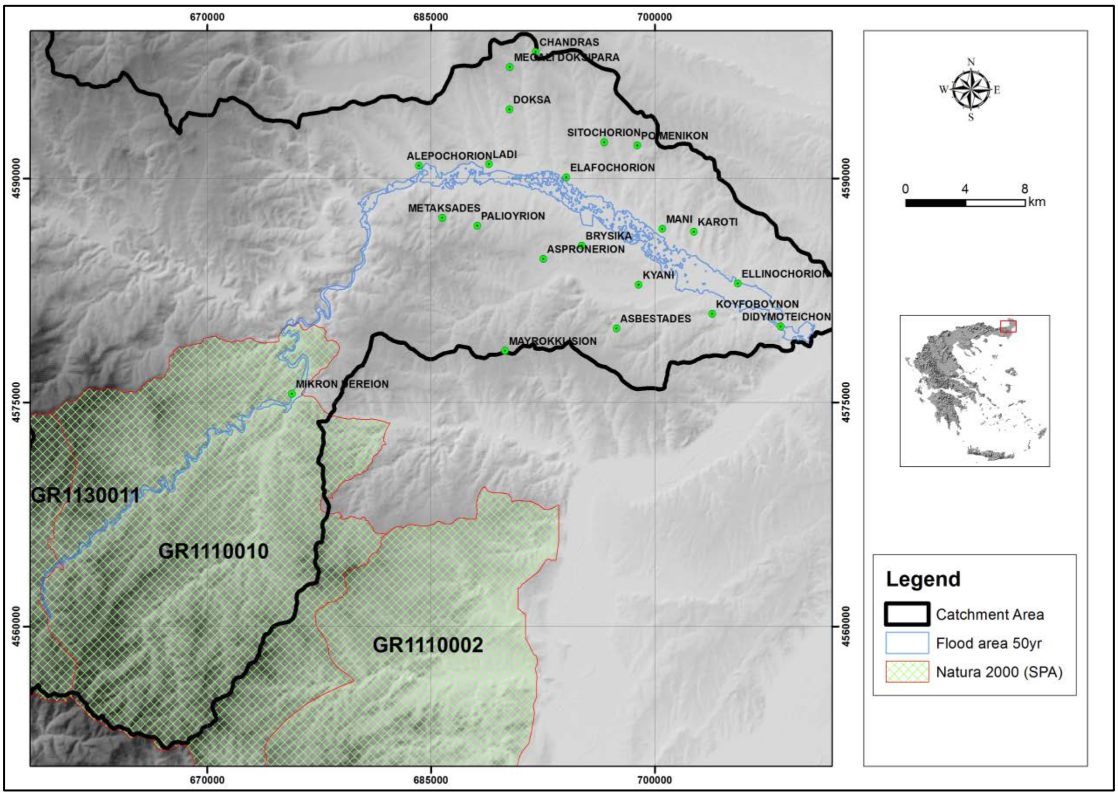

Figure 17: Flood risk map depicting the intersection between the inundated area of the 50 year period and Natura 2000 protected areas (GR1130011: Valley of Filiouri, GR1110010: Valley of Dereion).

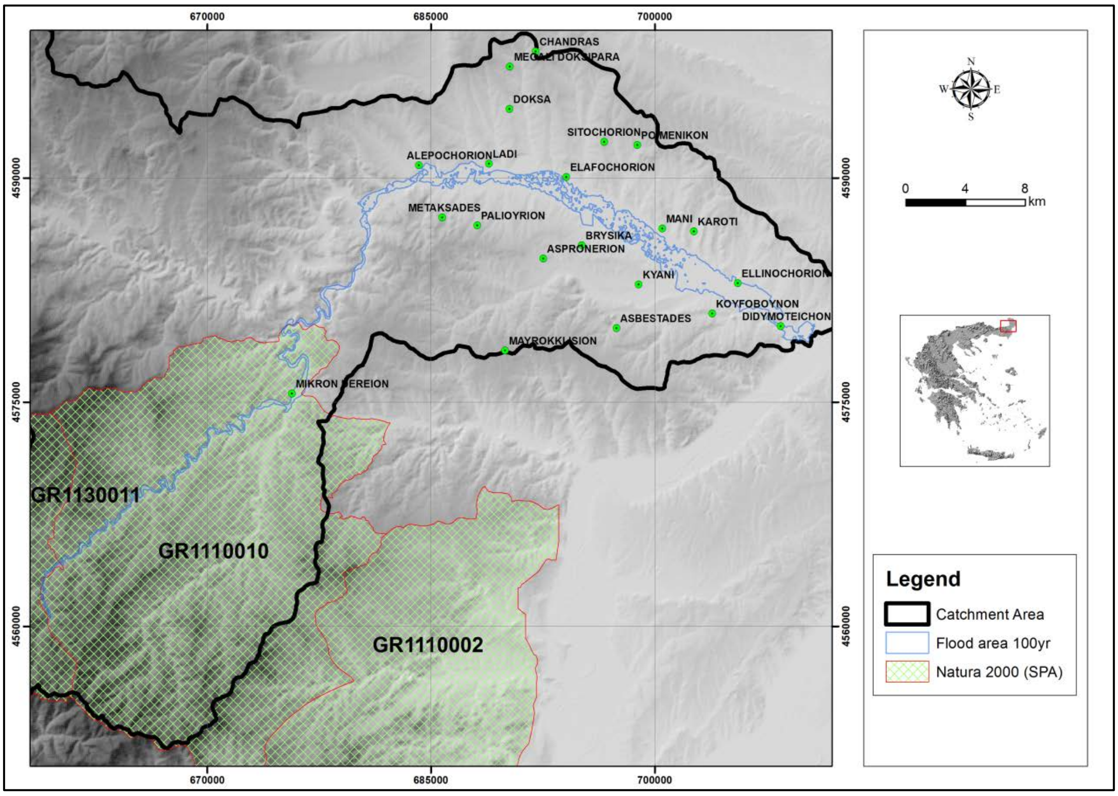

Figure 18: Flood risk map depicting the intersection between the inundated area of the 100 year period and Natura 2000 protected areas (GR1130011: Valley of Filiouri, GR1110010: Valley of Dereion).

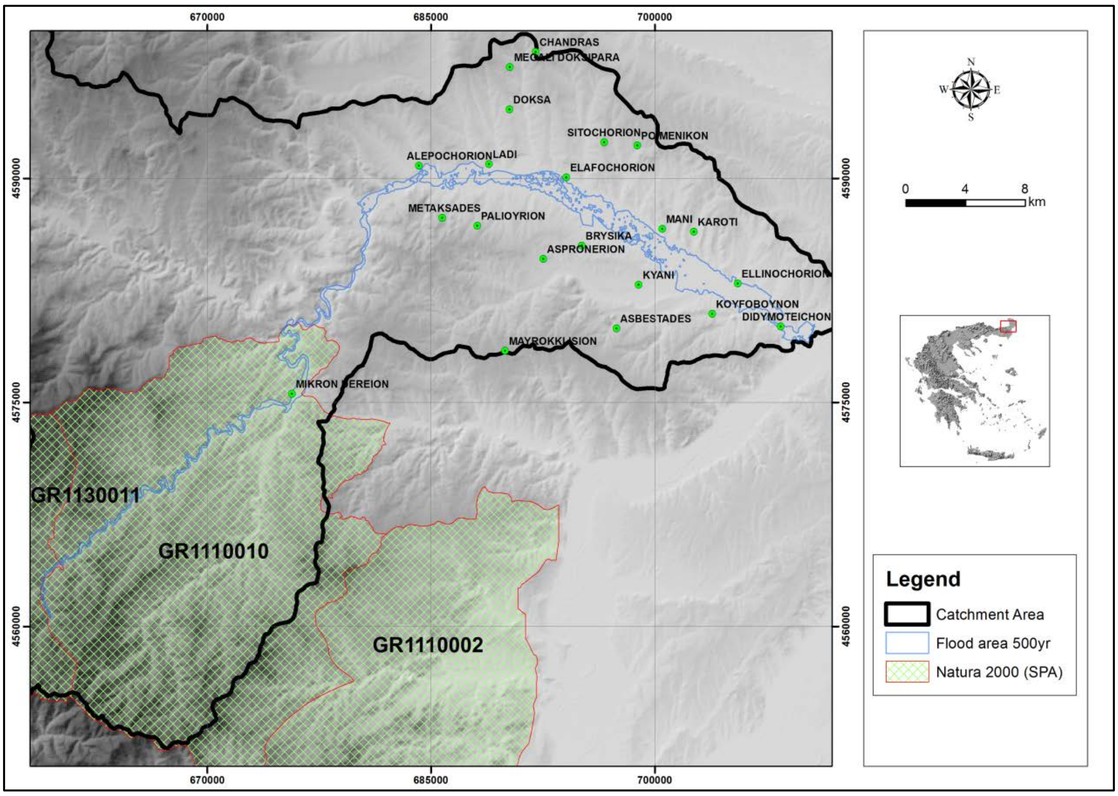

Figure 19: Flood risk map depicting the intersection between the inundated area of the 500 year period and Natura 2000protected areas (GR1130011: Valley of Filiouri, GR1110010: Valley of Dereion).

5. Discussion

The fact that the ENVISAT/ASAR images were of VV (Vertical -Vertical) polarisation proved satisfactory in detecting the flooded area (Horritt et al., 2002; Matgen et al., 2007; Hostache et al., 2012), according to the resulting false color multitemporal radar image. Thus, the methodology that was followed for floodplain delineation lies in accordance with the existing literature on flood monitoring, which claims that (smooth surface), copolarization (HH or VV) is preferred over cross-polarization (VH or HV) for flood mapping. Moreover, meteorological conditions can affect a SAR image that will be used for flood delineation, so it is important to obtain information that will help to gain knowledge upon the meteorological and hydrological conditions that are manifest during the SAR image's date and time of acquisition.

It appears that precipitation water is concentrated mostly upon augen gneisses. Also, the percentage ratio of the flooded area that is located upon the latter formation (41.31%) is greater than the percentage ratio of the total extent of the study area that is covered by it (30.96%). Furthermore, although 5.95% of the study area consists of Holocene sediments, approximately 13% of the total area extent of the study area is located upon that geological formation. Finally, it has to be mentioned that augen gneiss, Holocene sediments, sandstone (of marl-clay phase) and the formation that consists of pegmatites, marbles and amphibolites comprise 78.75% of the study area and are all considered impermeable geological formations.

Theresulting flood hazard maps indicate the existence of high flood depths near the village Mikron Dereion, where a water dam has been built, and NW of Didymoteicho. Also, an increase in flood depth and area extent as the return period increases, while the same appears to be true for the risk maps regarding the area that is common between the areas that were predicted by the hydraulic model that was produced by HEC-RAS and the Special Protection Areas (SPA) that belong to Natura 2000 Network. On the other hand, the measure of fit F, although very low in all cases, appears to be higher for the return period of 5 years indicating that the area of extent of a hydrologically modelled flooded area does not affect its predictive accuracy.

At this point, it has to be mentioned, that this study suggests that flood hazard and risk mapping, which are important tools according to 2007/60/EC Directive in flood hazard assessment and management can be achieved for river main watercourses at practically no cost if the materials that were used are taken under consideration. Surely, materials of better quality would greatly increase the accuracy and detail of the results, such as a DEM with better spatial resolution, but an overall realistic assessment of flood hazard can be achieved without them.

6. Conclusions

It appears that ESA's methodology on floodplain delineation via SAR imagery can produce satisfactory results provided that the appropriate "archive image" is selected. Gauge station data can be used in order to select such an image by excluding SAR images that were acquired during unfavourable weather conditions, for example during wind speed of more than 1.5 m/s.

It seems like flooded areas tend to be located upon impermeable geological formations, which is natural. However, despite the fact that, although 5.95% and 17.84% of the study area consists of Holocene sediments and sandstone (of marl-clay phase) respectively, approximately 13% of the total area extent of the inundated area is located upon the former and 5.07% upon the latter, perhaps indicates that flooded areas favour certain types of lithology. This connection, if it really exists, needs to be further examined and susceptibility mapping, regarding flood events, may prove a useful tool in achieving that.

The measures of fit test results indicate that the hydrologically modelled area of inundation does not correspond well with the flooded area that was observed by the SAR imagery. This can be attributed to the DEM's spatial resolution of 1 arc second (approximately 25 m), as coarser inaccurate topography produces in hydraulic simulations larger inundation extents (Cook, 2009). Also, it is worth to mention that the distribution of the flooded area as observed by the SAR imagery appears to be widespread throughout the catchment of Erythropotamos River and this can lead us to the conclusion that the whole of the drainage network is important when it comes to inundation area prediction via hydrological modelling, not only the main water course. Additionally, 1D hydrological modelling does not take under consideration rainfall intensity, which according to Costa (1987) is the second most important factor affecting peak discharge. Other types of maps, such as susceptibility maps, take under consideration the preparatory factors of a natural hazard (Domakinis, 2008), and it has to be examined if they can help to improve the accuracy of flood risk and hazard mapping as it was carried out by the methodology that was presented in this study.

Finally, it has to be mentioned that this is a preliminary study and the issues that were addressed in it will be ameliorated with the use of more detailed data layers, such as a DEM with better spatial resolution, and the introduction of additional factors, such as rainfall, with the aid of susceptibility mapping.

References

Alcantara – Ayala I., Goudie A., 2010. Geomorphological hazards and disaster prevention. Cambridge University Press, New York, 111-128.

Bates P.D., 2004. Remote sensing and flood inundation modeling. Hydrol. Processes 18, 2593–2597.

Bates P. D., Roo A.P.J., 2000. A simple raster-based model for flood inundation simulation. Journal of Hydrology 236, 54-77.

Bezes K. A., 1994. Interaction between surface water and groundwater in the valley of Evros' tributary Erythropotamos. Application of the mathematical model BEMERMHN.Proceedings of the 2nd Hydrogeological congress, Patras, 749-767 [in Greek with English abstract].

Cook A., Merwade V., 2009. Effect of topographic data, geometric configuration and modeling approach on flood inundation mapping. Journal of Hydrology 377, 131-142.

Costa J., 1987. Hydraulics and basin morphometry of the largest flash floods in the conterminous United States. Journal of Hydrology 93, 313-338.

Cunjian Y., Yiming W., Siyuan W., Zengxiang Z., Shifeng H., 2001. Extracting the flood extent from satellite SAR image with the support of topographic data. Procof IntConf on Inf Tech and InfNetworks (ICII 2001) 1, 87–92.

Csornai G., Suba Z., Nádor G., László I., CsekőÁ., Wirnhardt Cs., Tikász L., Martinovich L., 2004. Evaluation of a remote sensing based regional flood/waterlog and drought monitoring model utilising multi-source satellite data set including ENVISAT data. In: Proc. of the 2004 ENVISAT & ERS Symposium (Salzburg, Austria, 6–10 September 2004).

Dellepiane S., De Laurentiis R., Giordano F., 2004. Coastline extraction from SAR images and a method for the evaluation of the coastline precision. Pattern Recogn Lett 25:1461–1470.

Dewan A. M., Islam M. M., Kumamoto T., Nishigaki, M., 2007. Evaluating flood hazard for land use planning in Greater Dhaka of Bangladesh using remote sensing and GIS techniques. Water Resource Management 21, 1601–1612.

Dikau R., 1989. The application of a digital relief model to landform analysis. In: Three Dimensional Application in Geographical Information Systems, J.F. Raper (ed.), 51-77 (London: Taylor and Francis).

Domakinis C, Oikonomidis D, and Astaras T., 2008. Landslide mapping in the coastal area between the Strymonic Gulf and Kavala (Macedonia, Greece) with the aid of remote sensing and geographical information systems. International Journal of Remote Sensing 2008; 29:23, p. 6893-6915.

European Space Agency (E.S.A.), 2008. Radar Flood Mapping. Retrieved 6/2/2008 from: http://earth.eo.esa.int/download/eoedu/Earthnet-website-material/to-access-from -Earthnet/2010_AndeSAT-practical-sessions_Bolivia/NEST-processing_flood-mapping.pdf

European Space Agency (E.S.A.), 2014. EU-DEM. Retrieved 15/6/2014 from: http://www.eea.europa.eu/data-and-maps/data/eu-dem

Gan T. Y., Zunic F., Kuo C.-C., Strobl T., 2012. Flood Mapping of Danube River at Romania using single and multi-date ERS2-SAR images. International Journal of Applied Earth Observation and Geoinformation, 18, 69-81.

Hendrickx J.M.H., Remke L. van D., Borchers B., Curtis J., Lensen H. A., Harmon R., 2003. Worldwide distribution of soil dielectric and thermal properties. In: Proceedings of SPIE – The International Society for Optical Engineering (SPIE).

Hess L.L., Melack J.M., Solange F., Wang Y., 1995. Delineation of Inundated area and vegetation along the Amazon floodplain with the SIR-C Synthetic Aperture Radar. IEEE Trans. Geosci. Remote Sensing 33 (4), 896–905.

Horritt M.S., 1999. A statistical active contour model for SAR image segmentation. Image Vision Comput. 17 (3–4), 213–224.

Horritt M.S., 2006. A methodology for the validation of uncertain flood inundation models. J. Hydrol. 326, 153–165.

Horritt M. S., Bates P. D., 2002. Evaluation of 1D and 2D numerical models for predicting flood inundation. Journal of Hydrology 268, 78-99.

Hostache R., Lai X., Monnier J., Puech C., 2010. Assimilation of spatially distributed water levels into a shallow-water flood model. Part II: Use of a remote sensing image of Mosel River. Journal of Hydrogeology 390, 257-268.

Hostache R., Matgen P., Wagner W., 2012. Change detection approaches for flood extent mapping: How to select the most adequate reference image from online archives. Interantional Journal of Applied Earth Observation and Geoinformation 19, 205-213.

Hudson F. P., Colditz R. R., 2003. Flood delineation in a large and complex alluvial valley, lower Panuco basin, Mexico. Journal of Hydrology 280, 229-245.

Islam M., Sado K., 2000. Flood hazard assessment for the construction of flood hazard map and land development priority map using NOAA/AVHRR data and GIS – a case study in Bangladesh. Hydrological Sciences – Journal – des Sciences Hydrologiques 45 (3), 337–357.

Jodouin S., Bentabeta L., Zioua D., Vaillancourta J., Armenakis C., 2003. Spatial database updating using active contours for multispectral images: application with Landsat 7. ISPRS J. Photogrammetr. Remote Sensing 57, 346–355.

Kussul N., Shelestov A., Skakun S., 2008. Grid system for flood extent extraction from satellite images. Earth Science Informatics 1, 105-117., DOI 10.1007/s12145-008-0014-3, Springer-Verlag.

Lowry R. T., Langham E. J. & Mudry N., 1981. A preliminary analysis of SAR mapping of the Manitoba Flood, May 1979. Satellite Hydrology, American Water Resource Association, 316−323.

Marti-Cardona B., Lopez-Martines C., Dolz-Ripolles J., Blade-Castellet E., 2010.ASAR polarimetric, multi-incidence angle and multitemporal characterization of Donana Wetlands for flood extent monitoring.Remote Sensing of Environment 114, 2802-2815.

Martinez J. M., Le Toan T., 2007. Mapping of flood dynamics and spatial distribution of vegetation in the Amazon floodplain using multitemporal SAR data. Remote Sens Environ 108: 209–223.

Matgen P., Schumann G., Henry J.-B., Hoffmann L., Pfister L., 2007. Integration of SAR-derived inundation areas, high precision topographic data and ariver flow model toward

near real-time flood management. International Journal of Applied Earth Observation and Geoinformation 9, 247-263.
Mouratidis A., 2011. CEOGIS-floods: Contribution of Earth Observation data and GIS to mapping and managing flood evens in Greece. Final Report.Frascati, Italy, 7-20.
Mouratidis A., Ampatzidis D. European Digital Elevation Model (EU-DEM) validation against extensive Global Navigation Satellite Systems data and comparison with SRTM and ASTER-GDEM in Central Macedonia (Greece) [in press].
Niedermeier A., RomaneeßenE., Lenher S., 2000. Detection of coastline in SAR images using wavelet methods. IEEE Trans Geosci Remote Sens 38(5), 2270–2281.
Prigent C., Papa F., Aires F., Rossow W.B., Matthews E., 2007. Global inundation dynamics from multiple satellite observations, 1993–2000. J. Geophys. Res. 112, D12107.
Pulvirenti L., Chini M., Pierdicca N., Guerriero L., Ferrazzoli P., 2011. Flood monitoring using multi-temporal COSMO-SkyMed data: Image segmentation and signature interpretation.Remote Sensing of Environment (115), 990–1002.
Sanyal J., Lu, X.X., 2004. Application of remote sensing in flood management with special reference to Monsoon Asia: a review. Natural Hazards 33, 283–301.
Sarma P., 1999. Flood risk zone mapping of Dikrong sub basin in Assam. In: Proceedings of Map India Conference. New Delhi, 24–26 August.
Smith K., Petley D., 2009. Environmental Hazards: Assessing risk and reducing disaster. Routledge Taylor and Francis Group, London & New York, 232-261.
Soulios G., 1996. General Hydrogeology. University Studio Press, Thessaloniki, 50-75 [in Greek].
Suriya S., Mudgal B. V., 2012. Impact of urbanization on flooding: The Thirusoolam sub watershed – A case study. Journal of Hydrology 412-413, 210-219.
USGS (United States Geological Survey), 2011. Global Visualization Viewer (CLOVIS). Retrieved 15/4/2011 from: http://glovis.usgs.gov/
Voudouris, K., Mavrommatis, T., Antonakos, A., 2007. Hydrologic balance estimation using GIS in Korinthia prefecture, Greece. Advances in Science and Research 1, 1-8.
Wang Y., 2002. Mapping extent of floods: what we have learned and how we can do better. Natural Hazards Rev 3(2), 68–73.
Wang Y., Koopmans B.N., Pohl C., 1995. The 1995 flood in the Netherlands monitored from space – a multi-sensor approach. Int. J. Remote Sensing 16 (15), 2735–2739.
Wolman M.G., 1971. Evaluating alternative techniques of floodplain mapping. Water Resources Research 7, 1383-1392.